Preparation, Structural, and Electrical Studies of Polyaniline/$ZnFe_2O_4$ Nanocomposites

Gunderi Dhananjaya Prasanna,[1] Halepoojar Siddalingappa Jayanna,[1] Vishnu Prasad[2]

[1]*Department of Physics, Kuvempu University, Shankarghatta 577 451, Karnataka, India*
[2]*Department of Physics, Indian Institute of Science, Bangalore 560 012, Karnataka, India*

Received 12 February 2010; accepted 27 August 2010
DOI 10.1002/app.33304
Published online 10 January 2011 in Wiley Online Library (wileyonlinelibrary.com).

ABSTRACT: Polyaniline/$ZnFe_2O_4$ nanocomposites were synthesized by a simple and inexpensive one-step *in situ* polymerization method in the presence of $ZnFe_2O_4$ nanoparticles. The structural, morphological, and electrical properties of the samples were characterized by wide angle X-ray diffraction (WAXD), Fourier transform infrared (FTIR) spectroscopy, scanning electron microscopy (SEM), and thermogravimetric analysis (TGA). WAXD and SEM revealed the formation of polyaniline/$ZnFe_2O_4$ nanocomposites. Infrared spectroscopy indicated that there was some interaction between the $ZnFe_2O_4$ nanoparticles and polyaniline. The dc electrical conductivity measurements were carried in the temperature range of 80 to 300 K. With increase in the doping concentration of $ZnFe_2O_4$, the conductivity of the nanocomposites found to be decreasing from 5.15 to 0.92 Scm^{-1} and the temperature dependent resistivity follows ln $\rho(T) \sim T^{-1/2}$ behavior. The nanocomposites (80 wt % of $ZnFe_2O_4$) show a more negative magnetoresistance compared with that of pure polyaniline (PANI). These results suggest that the interaction between the polymer matrix PANI and zinc nanoparticles take place in these nanocomposites. J Appl Polym Sci 120: 2856–2862, 2011

Key words: conducting polymers; polyaniline; $ZnFe_2O_4$; nanocomposites; FTIR; conductivity

INTRODUCTION

The discovery of polymers has given a new dimension to the present era. Polymers are known so far as a class of heat sensitive, flexible, electrically insulating semicrystalline, or amorphous materials. A large number of polymers have been added to the list of conducting polymers such as polyaniline, polypyrrole, polythiophene, polyparaphenylene, polyphenylene sulfide, polyphenylene vinylene, etc. Polyaniline (PANI) exists in a variety of forms that differ in chemical and physical properties.[1,2] The most common green protonated emeraldine has a conductivity that of a semiconductor to the order of 100 Scm^{-1}. This is many orders of magnitude higher than that of common polymers ($<10^{-9}$ Scm^{-1}) and lower than that of typical metals ($>10^4$ Scm^{-1}).[3]

Many conducting polymers can be used as the conducting part of the composite material, such as PANI,[4,5] polypyrrole,[6,7] polythiophene,[8] polyacetylene, and their derivatives. Among all kinds of the conducting polymers, PANI is unique and has attracted much attention primarily due to its chemical and environmental stability,[9] being lightweight and having low cost, its facile synthetic process, and its readily controlled doping level.[10] PANI is electrically conducting and appears to be the ideal candidate for various applications. Many of their properties circumvent problems prevalent with traditional random access memory (RAM) (ferrites, carbon black), including corrosion, weight, matrix incompatibility, and environmental integrity.[11] In addition to being the corrosion resistant and light weight, many critical properties of PANI may be tailored for various applications. The strength to weight and the resistance to corrosion of PANI is the additional advantage over metals.

The PANI composites containing Fe_3O_4 nanoparticles are mostly studied for their electrical and magnetic characteristics. Among magnetic materials, the spinel ferrites exhibit remarkable magnetic properties particularly in radiofrequency region, physical flexibility, high electrical resistivity, mechanical hardness, and chemical stability.[12] Their properties are particularly enhanced when the size of the particles reaches the nanometer range.[13] $ZnFe_2O_4$ is an important magnetic ferrite which has been found its extensive applications in diverse areas such as permanent magnets, recording media, ferrofluids, and gas sensors. A number of articles have been published on the conducting and magnetic polymeric nanocomposites of polyaniline as well as polypyrrole

Correspondence to: H. S. Jayanna (jayanna60@gmail.com).

composites containing nanoparticles such as Fe_3O_4,[4,14] $NiFe_2O_4$,[9,15] $LiNiFe_2O_4$,[16] $MnZnFe_2O_4$,[17] $NiZnFe_2O_4$,[18] Fe_2O_3, $CoFe_2O_4$, Co_3O_4.

Although many articles on the nanocomposites of PANI with magnetic nanoparticles have been published recently,[19,20] there are few reports dealing with PANI/$ZnFe_2O_4$ nanocomposites.[21] In the present work, $ZnFe_2O_4$ nanoparticles were prepared by citrate-nitrate method and PANI/$ZnFe_2O_4$ nanocomposites were synthesized by *in situ* polymerization of aniline in the presence of $ZnFe_2O_4$ nanoparticles. This approach provides a one-step, simple, and inexpensive method for the preparation of PANI/$ZnFe_2O_4$ nanocomposite. The structural, morphological, and electrical properties of nanocomposites were characterized by wide angle X-ray diffraction (WAXD), Fourier transform infrared (FTIR) spectroscopy, scanning electron microscopy (SEM), and thermogravimetric analysis (TGA). The temperature dependence of dc resistivity on PANI/$ZnFe_2O_4$ nanocomposites was investigated in the temperature range 80–300 K.

EXPERIMENTAL

Preparation of $ZnFe_2O_4$

Zinc ferrite nanoparticles have been prepared by Sol-Gel citrate–nitrate method[22] using zinc nitrate and ferric nitrate in the ratio 1:2. To start with certain amount of citric acid is dissolved in distilled water, then $Zn(NO_3)_2.6H_2O$ and $Fe(NO_3)_3.9H_2O$ were dissolved in it with a molar ratio 1:1 of nitrate to citric acid. A small amount of ammonia was then added to the solution to adjust the pH value to 7 and stabilized the nitrate–citrate solution.[23] During this process the solution was continuously stirred at a constant temperature of 80°C. Then, the stabilized nitrate-citrate solution was poured into a Petri dish and then heated slowly up to 120°C. The viscosity and color of the solution during heating changed into brown, puffy, porous dry gel. When the temperature of the gel was raised to 250°C, the dried gel suddenly catches fire and then burn in self-propagation combustion manner until it was completely transformed into foam powder. The foam powder was then ground into fine powder. The resultatnt $ZnFe_2O_4$ nanoparticles were dried at 150°C for 12 h in hot air oven.

Preparation of polyaniline/$ZnFe_2O_4$ nanocomposite

Polyaniline/$ZnFe_2O_4$ nanocomposites were prepared by a simple *in situ* polymerization method[3,24] in the presence of $ZnFe_2O_4$ nanoparticles. Zinc Ferrite nanoparticles (20 wt %, 40 wt %, 60 wt %, and 80 wt %) were added to 100 mL of 1*N* HCl solution containing 2 g of aniline monomer and stirred for 30 min to disperse the aniline homogenously. A precooled solution containing 4.56 g (0.2*M*) of ammonium per sulphate $[(NH_4)_2.S_2O_8]$ in 100 mL of 1*N* HCl solution was then slowly added drop wise to the suspension mixture by constant stirring which is maintained at 0–5°C. The polymerization was allowed to proceed for 8–10 h at temperature 0–5°C. The reaction mixture was then left in a freezer overnight and filtered. The nanocomposites were obtained by filtering and washing the suspension with methanol and deionized water repeatedly until the filtered solution became colorless, and dried under vacuum at 80°C for 24 h. The dried polymer was ground into a fine powder. Different PANI/$ZnFe_2O_4$ composites were synthesized using 0, 20, 40, 60, and 80 wt % of $ZnFe_2O_4$ with respect to aniline monomer.

Characterization

Wide angle X-ray diffraction (WAXD) pattern of the samples was collected on a Philips X'pert Pro MPD X-ray diffractometer with Cu-K_α radiation (λ = 1.5418 Å) at a scanning rate of 0.05° per step with 15 s/step in the range of 10–80°. The average crystalline size of $ZnFe_2O_4$ was determined by Debye-Scherrer's equation given by,

$$d = \frac{0.89\ \lambda}{\beta \cos\theta}$$

where d is the size of the particle, λ the X-ray wavelength, β the full width half maxima expressed in unit of 2θ, and θ is the Bragg's angle,

FTIR spectroscopy were recorded on a PERKIN-ELMER (model-1000) spectrometer in the range of 400–2500 cm^{-1} using KBr pellets. Scanning Electron Micrograph (SEM) was carried out in a Hitachi model *S*-3200N microscope.

The DC electrical conductivity was carried by four probe method using Keithley source meter (model 220) and a multimeter (Model 2000) in the temperature range 80–300 K by using Lakeshore auto tuning temperature controller (Model-330). The samples were pressed into a pellet of thickness 1–2 mm and of diameter 10 mm. A thin copper wire act as leads and conducting silver paste was used for ohmic contacts. The measurements were recorded during cooling cycle. The electrical resistivity ρ was calculated by the formula,

$$\rho = V/I(A/t)$$

where V is the applied voltage, I the measured current, A the area of the pellet, and t the average distance between the probes.

The magneto resistance (MR) studies were carried out on a Janis make superconducting magnet liquid helium cryostat.

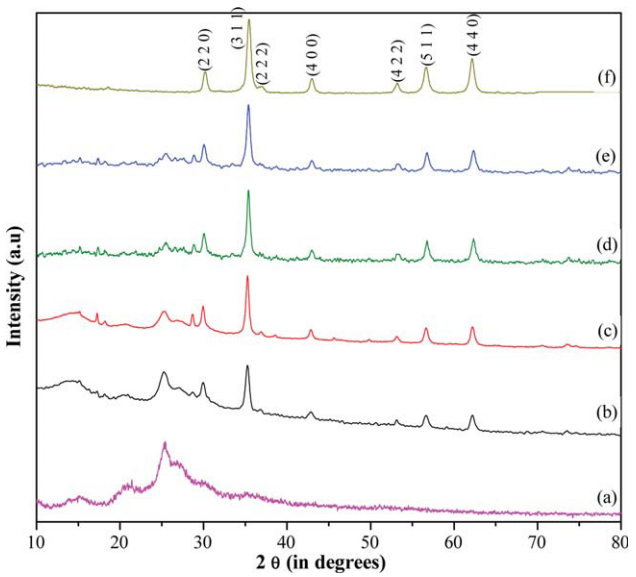

Figure 1 XRD patterns of (a) pure PANI, PANI/$ZnFe_2O_4$ nanocomposites containing: (b) 20 wt %, (c) 40 wt %, (d) 60 wt %, (e) 80 wt %, (f) pure $ZnFe_2O_4$ nanoparticles. [Color figure can be viewed in the online issue, which is available at wileyonlinelibrary.com.]

RESULTS AND DISCUSSION

WAXD

Wide angle X-ray diffraction pattern for polyaniline and nanocomposites samples with increasing content of $ZnFe_2O_4$ were presented in Figure 1. Diffraction pattern for $ZnFe_2O_4$ nanoparticles [Fig. 1(f)] shows a cubic spinel phase with fcc structure (JCPDS card No. 82-1042) with no extra reflections and are well indexed to the crystallographic planes of spinel ferrite (220), (311), (222), (400), (422), (511), and (440) with 100% intensity at $2\theta = 34.87^\circ$ that corresponds to the reflection plane (311). The average particle size was determined by Debye-Scherrer's formula and for pure $ZnFe_2O_4$ it is found to be 20 nm; and increases with decreasing content of $ZnFe_2O_4$ in PANI. It is also evident from the Figure 1 that, the pure polyaniline has broad peak [Fig. 1(a)] in the region of 20–30° with a maximum at around 25° indicating its semicrystalline nature. In the Figure 1(b–f), with increasing content of $ZnFe_2O_4$ nanoparticles in the composite the relative intensity of the characteristic peaks of PANI/$ZnFe_2O_4$ nanocomposites increase regularly, clearly indicating an increase in the $ZnFe_2O_4$ content in nanocomposites.

FTIR

Figure 2 shows the FTIR spectroscopy of pure polyaniline, polyaniline/$ZnFe_2O_4$, and pure $ZnFe_2O_4$ nanoparticles. The characteristic peaks of PANI occur at 1563, 1483, 1298, 1242, 1143, and 800 cm^{-1}.[15] The peaks at 1563 and 1483 cm^{-1} are attributed to the characteristic C=C stretching of the quinoid and benzenoid rings, the peaks at 1298 and 1242 cm^{-1} are assigned to C-N stretching of the benzenoid ring, the broad peak at 1143 cm^{-1} which is described by Ahmad et al.[25] as the "electronic-like band" is associated with vibration mode of N=Q=N, indicating that HCl doped PANI is formed in our samples, and the peak at 800 cm^{-1} for PANI is attributed to the out of-plane deformation of C-H in the 1,4-disubstituted benzene ring.[18]

In ferrites, the metal ions are situated in two different sublattice, designated tetrahedral and octahedral according to the geometrical configuration of the oxygen nearest neighbors.[16] From Figure 2 we can see that the spectroscopy for PANI and PANI/$ZnFe_2O_4$ are similar and the characteristic peak value of PANI at 1143 and 1483 cm^{-1} in Figure 2(a). The peaks of the PANI/$ZnFe_2O_4$ nanoparticles shift to lower wave numbers. This indicates that the PANI/$ZnFe_2O_4$ powders are composed of $ZnFe_2O_4$ nanocomposites, which infer there is some interaction between $ZnFe_2O_4$ particles and PANI backbone. Peak assignment of PANI and PANI/$ZnFe_2O_4$ nanocomposites were given in Table I.

SEM

The morphology and particle sizes of polyaniline/$ZnFe_2O_4$ nanocomposites were determined by SEM. The typical SEM micrographs of $ZnFe_2O_4$ nanoparticles are shown in Figure 3(a) exhibiting spherical morphology with particle size in the range of 80–100 nm. Polyaniline/$ZnFe_2O_4$ nanocomposites (60 wt %) are shown in Figure 3(b). The SEM micrograph reveals that polyaniline is deposited on the surface

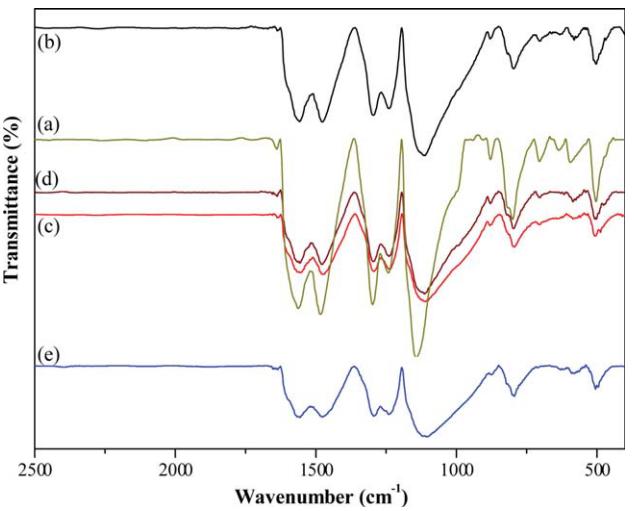

Figure 2 FTIR spectroscopy of (a) pure PANI, PANI/$ZnFe_2O_4$ nanocomposites containing: (b) 20 wt %, (c) 40 wt %, (d) 60 wt %, (e) 80 wt % $ZnFe_2O_4$ nanoparticles. [Color figure can be viewed in the online issue, which is available at wileyonlinelibrary.com.]

TABLE I
FTIR Peaks of PANI and PANI/$ZnFe_2O_4$ Nanocomposites

Wave number (cm^{-1})			
Pure PANI	$ZnFe_2O_4$ (20 wt %)	$ZnFe_2O_4$ (40 wt %)	Peak assignment
1563	1558	1555	C=C stretching of quinoid rings
1483	1476	1471	C=C stretching of benzenoid rings
1298, 1242	1295, 1240	1293, 1237	C-N stretching of the benzenoid ring
1143	1111	1112	C-H in-plane bending modes
800	797	794	C-H out-of-plane bending modes

of $ZnFe_2O_4$ particles and it is indicated that the nanocomposites are composed of polycrystalline ferrite particles and PANI, which is in accordance with the results by WAXD analysis. It also indicates that most of the $ZnFe_2O_4$ particles are finely dispersed in the PANI matrix, a very few particles are clumped. In fact, it is the polymer matrix that plays the role of minimizing the aggregation of nanoparticles

TGA

The TGA curve of PANI and PANI/$ZnFe_2O_4$ composites are shown in Figure 4. For pure PANI in Figure 4(a) the first weight losses below 100°C were presumably a result of the water or hydrogen chloride released from the sample. A gradual weight loss for PANI, which began at about 220°C and continued to 750°C, was attributed to the degradation of PANI chains. The gradual weight losses are observed at the temperature above 200°C for all composites, revealing PANI itself was decomposed thermally within this temperature range, and PANI has the great weight lose (about 75%) at the temperature between 300°C and 700°C. Figure 4(b–e) shows the curves correspond to $ZnFe_2O_4$ concentrations of 20 wt %, 40 wt %, 60 wt %, and 80 wt %, respectively. The decomposition temperature of the PANI/$ZnFe_2O_4$ composites was found to depend on the amount of $ZnFe_2O_4$ nanoparticles present in the composite. The initial decomposition temperatures for 20 wt % and 40 wt % of $ZnFe_2O_4$ are at 200°C and 290°C respectively, whereas for 60 wt % and 80 wt % of $ZnFe_2O_4$ are found to be at 350°C and 400°C, respectively.

Electrical properties

The temperature dependent of resistivity of PANI/$ZnFe_2O_4$ composites with different $ZnFe_2O_4$ content was measured in the temperature range of 80 to 300 K. The resistivity of all measured samples increases with decreasing temperature exhibiting typical semiconducting behavior as shown in Figure 5. The room temperature conductivity for pure PANI is 5.15 Scm^{-1} and it decreases with increase in the $ZnFe_2O_4$ content.

It is found that the temperature dependence of resistivity of the PANI/$ZnFe_2O_4$ composites follows a $\ln \rho(T) \sim T^{-1/2}$ law (as shown in Fig. 6) similar to as reported by Long et al.[26] and it can be interpreted by quasi-one-dimensional variable. The temperature dependence of ρ_{dc} for disorder semiconductor is generally described by variable range hopping Model (VRHM).

$$\rho(T) = \rho_o \exp\left(\frac{T_o}{T}\right)^{1/(1+d)}$$

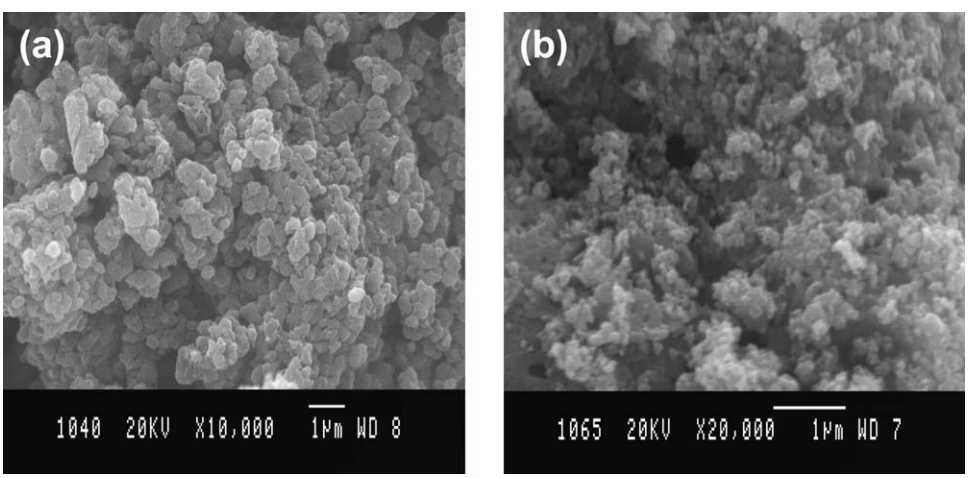

Figure 3 SEM images of (a) $ZnFe_2O_4$ and (b) PANI/$ZnFe_2O_4$ nanocomposites (60 wt %).

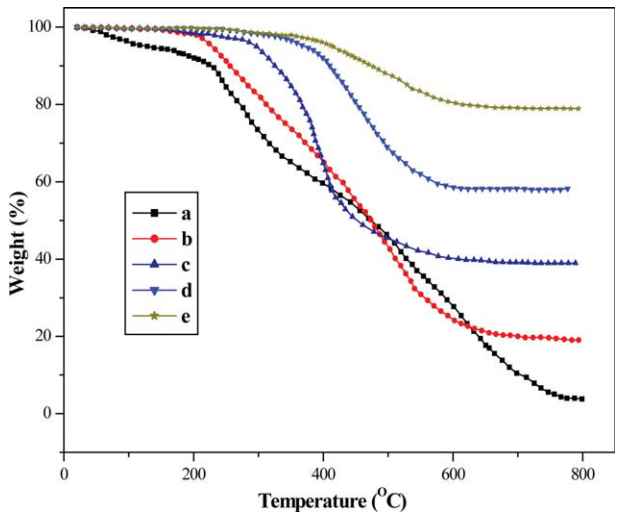

Figure 4 TGA thermograms of (a) pure PANI, PANI/$ZnFe_2O_4$ nanocomposites containing: (b) 20 wt %, (c) 40 wt %, (d) 60 wt %, (e) 80 wt % $ZnFe_2O_4$ nanoparticles. [Color figure can be viewed in the online issue, which is available at wileyonlinelibrary.com.]

where $d = 1$, 2, and 3 is connected with the effective dimensionality of the charge transport in the solid and T_0 is the characteristic Mott temperature. The smaller value of T_0 indicates the higher conductivity of the sample. The value of T_0 can be obtained from the slope of ln $\rho(T) \sim T^{-1/2}$ plot.

Since the $ZnFe_2O_4$ nanoparticles are embedded in the PANI matrix, interactions between the polymer matrix and $ZnFe_2O_4$ nanoparticles will increase the charge carrier scattering and thus increase the sample's resistivity resulting in decrease in the conductivity of PANI/$ZnFe_2O_4$ composites with increase in $ZnFe_2O_4$ content. Other effects like increased charge carrier trapping, either by the nanoparticles themselves or by morphological changes and defects induced by them, could also play a role. As shown in Figure 7, when the $ZnFe_2O_4$ content increases from 0 to 80 wt %, the characteristic Mott temperature T_0 increases from 31 to 95 K, while the room-temperature conductivities σ_{RT} decreases from 5.15 to 0.92 Scm^{-1}.

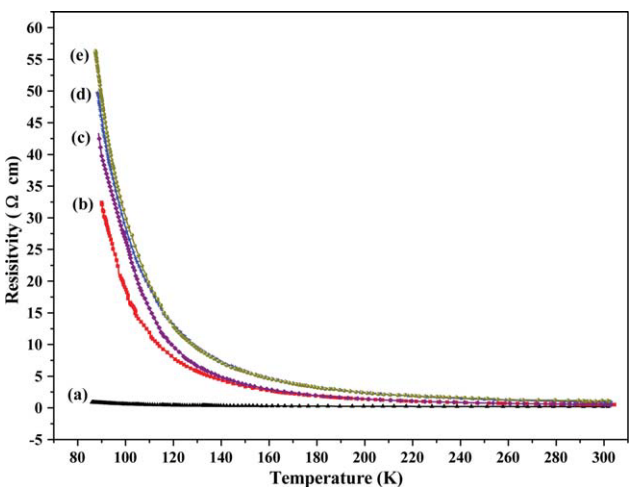

Figure 5 Temperature dependence of resistivity of (a) pure PANI, PANI/$ZnFe_2O_4$ nanocomposites containing: (b) 20 wt %, (c) 40 wt %, (d) 60 wt %, (e) 80 wt % $ZnFe_2O_4$ nanoparticles. [Color figure can be viewed in the online issue, which is available at wileyonlinelibrary.com.]

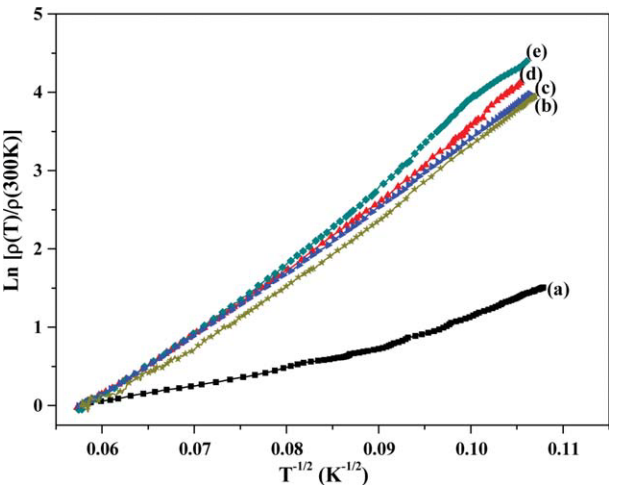

Figure 6 The variation of resistivity with $T^{-1/2}$ for (a) pure PANI, PANI/$ZnFe_2O_4$ nanocomposites containing: (b) 20 wt %, (c) 40 wt %, (d) 60 wt %, (e) 80 wt % $ZnFe_2O_4$ nanoparticles. [Color figure can be viewed in the online issue, which is available at wileyonlinelibrary.com.]

Magnetoresistance

As mentioned above, if the interactions between the supporting matrix and $ZnFe_2O_4$ nanoparticles are strong, it should be interesting to measure the electrical resistivity as a function of temperature with constant magnetic field. The magneto resistance (MR) for all samples was measured in the temperature range 30 to 300 K in the presence of magnetic

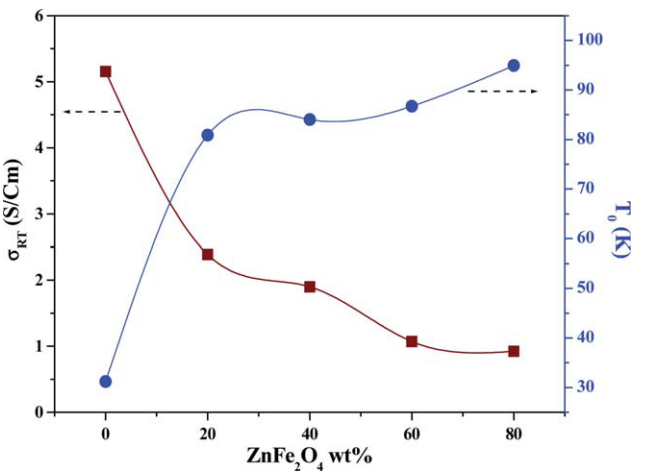

Figure 7 The variation of room temperature conductivity σ_{RT} and characteristic Mott temperature T_0 with $ZnFe_2O_4$ content. [Color figure can be viewed in the online issue, which is available at wileyonlinelibrary.com.]

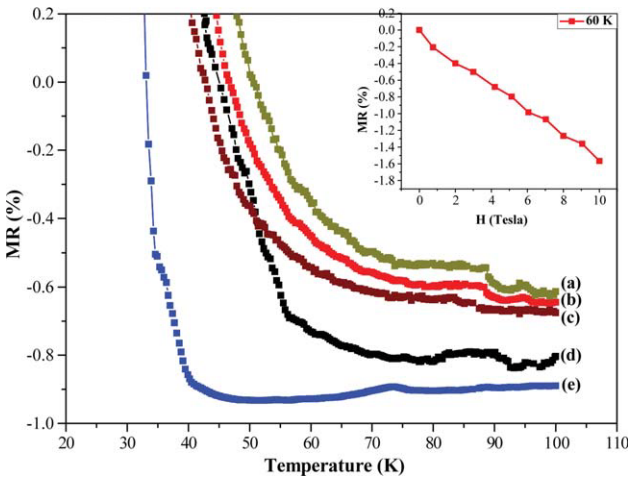

Figure 8 Temperature dependence of magnetoresistance (MR) of (a) pure PANI, PANI/$ZnFe_2O_4$ nanocomposites containing: (b) 20 wt %, (c) 40 wt %, (d) 60 wt %, (e) 80 wt % $ZnFe_2O_4$ nanoparticles, at $H = 2T$ (inset: MR of PANI at $T = 60$ K). [Color figure can be viewed in the online issue, which is available at wileyonlinelibrary.com.]

field 2T. The MR is defined as MR = [ρ(*H*)-ρ(0)]/ρ(0), where *H* is the applied magnetic field. Figure 8 shows the MR characteristics for all samples as a function of temperature. The MR of pure PANI is very small and negligible. It is obviously that the large MR of the composite is related with $ZnFe_2O_4$ nanoparticles. The inset figure shows the MR for pure PANI at 60 K which is very low. In the absence of any magnetic field, the resistivity of the composite increases with increasing $ZnFe_2O_4$ content due to increased charge carrier scattering. When a magnetic field is applied, the scattering between charge carriers and $ZnFe_2O_4$ particles is depressed (similar to the depression of the spin–flip scattering in the Kondo effect) in systems containing magnetic impurities.[15]

It is found that the MR increases with lowering of temperature, and around 30–60 K a transition from negative MR to positive MR was observed. A similar transition has been reported for PANI and polypyrrole nanostructures.[26,27] Below 35 K, the MR is positive for all samples and the magnitude increases sharply with decreasing temperature. So the resistivity decreases (negative MR), and the negative MR increases with increasing temperature from 30 to 60 K due to stronger depression and remains constant till 300 K (not shown in the Fig. 8). Figure 8 also shows the effect of the $ZnFe_2O_4$ on the low-temperature MR. With increasing $ZnFe_2O_4$ concentration, the negative contribution to the MR increases.[27] The above results indicate that there is a change of sign in the low-temperature MR with lowering temperature. The change of sign demonstrates that there are two kinds of contributions, namely, negative and positive contributions to the low-temperature MR, which are coexistent and competitive. When the positive contribution is larger than the negative contribution, a transition from negative MR to positive MR occurs. At low fields (2T), the phase between alternate hopping paths enclosing a magnetic flux is changed by the flux. This quantum interference effect leads to a negative MR. It is noted that Faran and Ovadyahu[28] have already pointed out that the negative MR in samples in the VRH regime is not strikingly different from the MR in the weak localization regime. Thus these results indicate that the MR is a function of temperature and $ZnFe_2O_4$ concentration.

CONCLUSIONS

Polyaniline/$ZnFe_2O_4$ nanocomposites were successfully synthesized via *in situ* polymerization of aniline in the presence of $ZnFe_2O_4$ nanoparticles. The result of FTIR spectroscopy, WAXD, and TGA shows the formation of the composite and indicate an interaction between PANI and $ZnFe_2O_4$. The conductivity of the nanocomposite decreases with increase in the doping concentration of $ZnFe_2O_4$ from 5.15 to 0.92 Scm^{-1}. The temperature dependent resistivity follows a ln ρ(*T*) $\sim T^{-1/2}$ law which exhibits semiconducting behavior and the characteristic Mott temperature T_0 increases from 31 to 95 K. The MR of pure PANI is small and more negative. On the other hand the MR of PANI/$ZnFe_2O_4$ nanocomposites are negative and large due to the depression of charge carrier scattering.

Authors are thankful to Department of Physics, Indian Institute of Science, Bangalore, for providing laboratory facilities.

References

1. Gospodinova, N.; Terlemezyan, L. Prog Polym Sci 1998, 23, 1443.
2. Trivedi, D. C. In Handbook of Organic Conductive Molecules and Polymers; Nalwa H. S., Ed.; Wiley Publishers: Chichester, 1997; Vol.2.
3. Stejskal, J. IUPAC technical report. Pure Appl Chem 2002, 74, 857.
4. Aphesteguy, J. C.; Silvia, E. J. J Mater Sci 2007, 42, 7062.
5. Jiang, J.; Ai, L. H. Mater Lett 2008, 62, 3643.
6. Mallouki, M.; Tran-Van, F.; Sarrazin, C.; Simon, P.; Daffos, B.; De, A.; Chevrot, C.; Fauvarque, J. F. J Solid State Electrochem 2007, 11, 398.
7. Alqudami, A.; Annapoorni, S.; Sen, P.; Rawat, R.S. Synth Met 2007, 157, 53.
8. Kousik, G.; Pitchumani, S., Renganathan, N. G. Prog Orga Coat 2001, 43, 286.
9. Zhong-Ai, H.; Hong-Xiao, Z.; Chao, K.; Yu-Ying, Y; Xiu-Li, S.; Li-Jun, R.; Yan-Peng, W. J Mater Sci Mater Electron 2006, 17, 859.
10. Huang, J.; Kaner, R. B. J Am Chem Soc 2004, 126, 851.
11. Faez, R.; Martin, I. M.; De Paoli, M. A.; Rezedene, M. C. Synth Met 2001, 119, 435.
12. Huang, X.; Chen, Z. Mater Res Bull 2005, 40, 105.
13. Kodama, R. H. J Magn Magn Mater 1999, 200, 359.
14. Long, Y.; Chen, Z.; Duvail, J. L.; Zhang, Z; Wan, M. Phys B: Condens Matter 2005, 370, 121.
15. Jiang, J. J Macromol Sci Phys 2008, 47, 242.
16. Jiang, J.; Li, L.; Xu, F. Mater Sci Eng A 2007, 456, 300.
17. Lee, S. P.; Chen, Y. J.; Ho, C. M.; Chang, C. P.; Hong, Y. S. Mater Sci Eng B 2007, 143, 1.

18. Li, G.; Yan, S.; Zhou, E.; Chen, Y. Colloids Surf A 2006, 276, 40.
19. Dea, A.; Senb, P.; Poddara, A.; Dasaet, A. Synth Met 2009, 159, 1002.
20. Reddy, K. R.; Park, W.; Sin, B. C.; Noh, J.; Lee, Y. J Colloid Interface Sci 2009, 335, 34.
21. Stejskal, J.; Trchova, M.; Brodinova, J.; Kalenda, P.; Fedorova, S. V.; Prokes, J.; Zemek, J. J Colloid Interface Sci 2006, 298, 87.
22. Hwang, C. C.; Wu, T. Y.; Wan, J.; Tsai, J. S. Mater Sci Eng B 2004, 111, 49.
23. Zhang, R.; Huang, J.; Zhao, J.; Sun, Z.; Wang,Y. Energy Fuels 2007, 21, 2682.
24. Singh, K.; Usha, M. E. Indian J Chem Sect A 2007, 36, 295.
25. Ahmad, N.; MacDiarmid, A. G. Synth Met 1996, 78, 103.
26. Long, Y.; Chen, Z.; Shen, J.; Zhang, Z.; Zhang, L.; Huang, K.; Wan, M.; Jin, A.; Gu, C.; Duvail, J. L. Nanotechnology 2006, 17, 5903.
27. Long, Y. Z.; Yin, Z. H.; Chen, Z. J. J Phys Chem C 2008, 112, 11507.
28. Faran, O.; Ovadyahu, Z. Phys Rev B: Condens Matter 38: 54571988.